Supplement of Nat. Hazards Earth Syst. Sci., 19, 837–856, 2019
https://doi.org/10.5194/nhess-19-837-2019-supplement

Natural Hazards and Earth System Sciences
Open Access
EGU

Supplement of

Simple rules to minimise exposure to coseismic landslide hazard

David G. Milledge et al.

Correspondence to: David G. Milledge (david.milledge@newcastle.ac.uk)

Supplementary Information 1: Hazard area performance with optimised, global and hold-back parameters

At each of the six study sites we optimise the two parameters in the SHALRUN-EQ model required to predict hazard area, initiation angle (θ_m) and stopping angle (θ_s), by sampling values for each parameter uniformly in 1 degree increments over the range [20,70] for initiation angle and [0,50] for stopping angle, and imposing the requirement: $\theta_m > \theta_s$. For our objective function, we use the area under the receiver operating characteristic (ROC) curve, comparing landslide hazard derived from hazard area to the inventory of observed landslides at each site. The optimisation surfaces are shown in Figure S1. To generalise our results, we then take arithmetic means of the optimum initiation and stopping angles, to generate hazard area predictions using a single 'global' rule averaged over all six inventories (Table S1). To remove the influence of test data on the test itself, we re-run the hazard area prediction for each inventory as a hold back-test, in which we re-calculate the initiation and stopping parameters excluding the optimised values from that inventory and using only the remaining five inventories.

We find that the differences in ROC curves (Figure S2) and area under the curve values (Table S1) are fairly subtle. Hazard area with global average parameters performs well overall, with AUC values that range from 0.78 to 0.86. Hazard area with parameters that are optimised for each inventory offers only a slight further improvement, with AUC increased by <3% in each case (Table S1). Optimised initiation and stopping angles can differ quite radically between sites, ranging from 31-45˚ for initiation angle and from 3-19˚ for stopping angle. This might signal cause for concern about how feasible it is to find a single general rule, given such variability in optimum parameters between sites. However, hazard area skill is relatively insensitive to parameter variation close to the optimum parameters, as indicated by the relatively smooth and gentle peaks of the optimisation surfaces in Figure S1. Thus, the (sometimes large) differences between global and optimised parameter values do not translate into large performance differences between hazard area predictions using global or optimised parameters. The use of hold-back rather than global parameters results in an even smaller difference in performance; AUC values are reduced by <1% for every inventory and hazard area is still the best metric at all sites. For this reason, we include hold-back tests here but report results from global average parameters rather than hold-back parameters in the paper for simplicity. It is

these global average parameters (initiation angle of 40° and stopping angle of 10° when rounded to one significant figure) that form the basis of our simple rule, and that we would recommend when applying the SHALRUN-EQ approach to a new location (in the absence of a landslide inventory with which to test and calibrate the parameters).

Table S1: Parameter values and areas under the ROC curve for the six inventories

	Parameters		Area Under ROC Curve		
	Initiation slope θ_i (˚)	Stopping slope θ_s (˚)	Hazard area optimised	Hazard area global	Hazard area holdback
Finisterre	34	19	0.91	0.89	0.88
Northridge	41	19	0.80	0.79	0.78
Chichi	44	4	0.80	0.80	0.79
Wenchuan	39	3	0.78	0.78	0.78
Haiti	31	9	0.88	0.86	0.85
Gorkha	45	6	0.89	0.88	0.88
Average	**39**	**10**	**0.84**	**0.83**	**0.83**
1σ	**6**	**7**	**0.1**	**0.1**	**0.1**

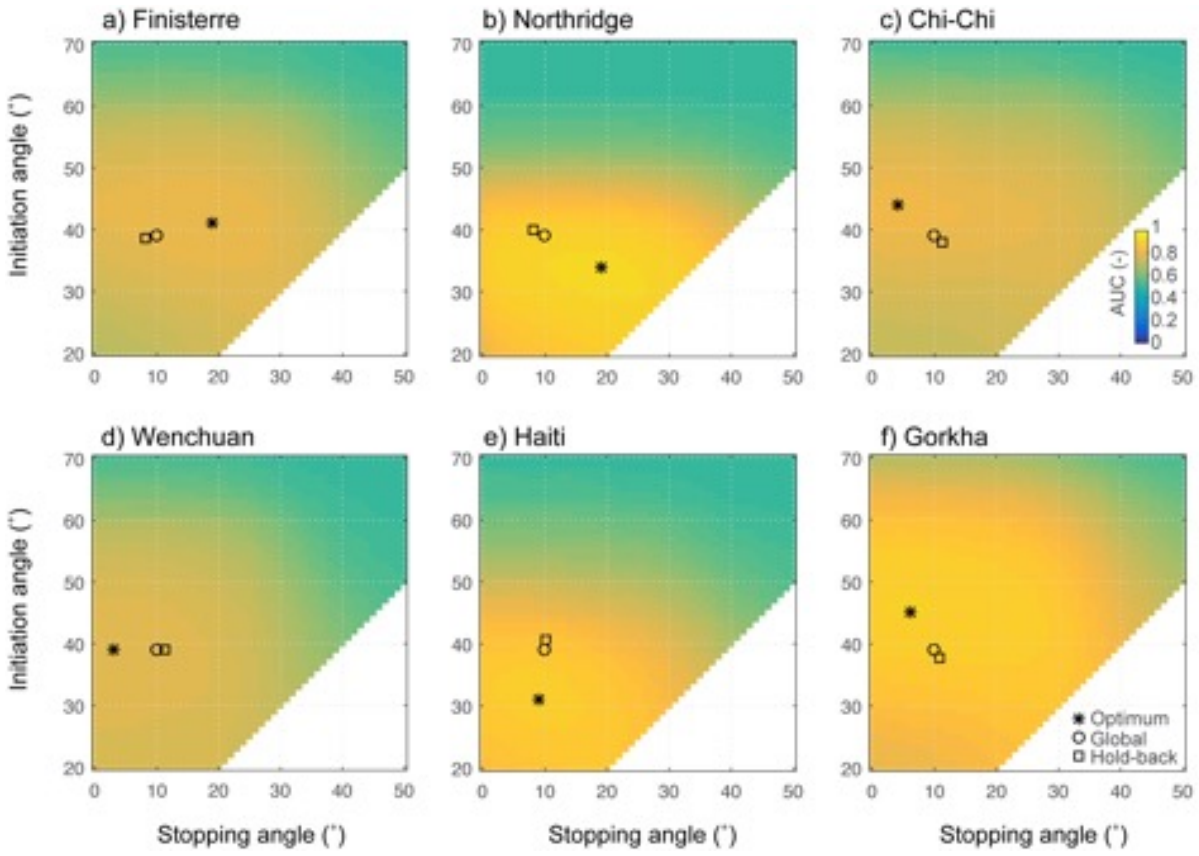

Figure S1: Model predictive skill for SHALRUN-EQ for each of the six landslide inventories across reasonable ranges for the two parameters, initiation angle (θ_m) and stopping angle (θ_s). Predictive skill is quantified using area under the receiver operating characteristic curve. The six inventories are: a) Finisterre, b) Northridge, c) Chi-Chi, d) Wenchuan, e) Haiti, f) Gorkha. Symbols show the parameter combinations from site specific optimisation, global average, and hold-back average.

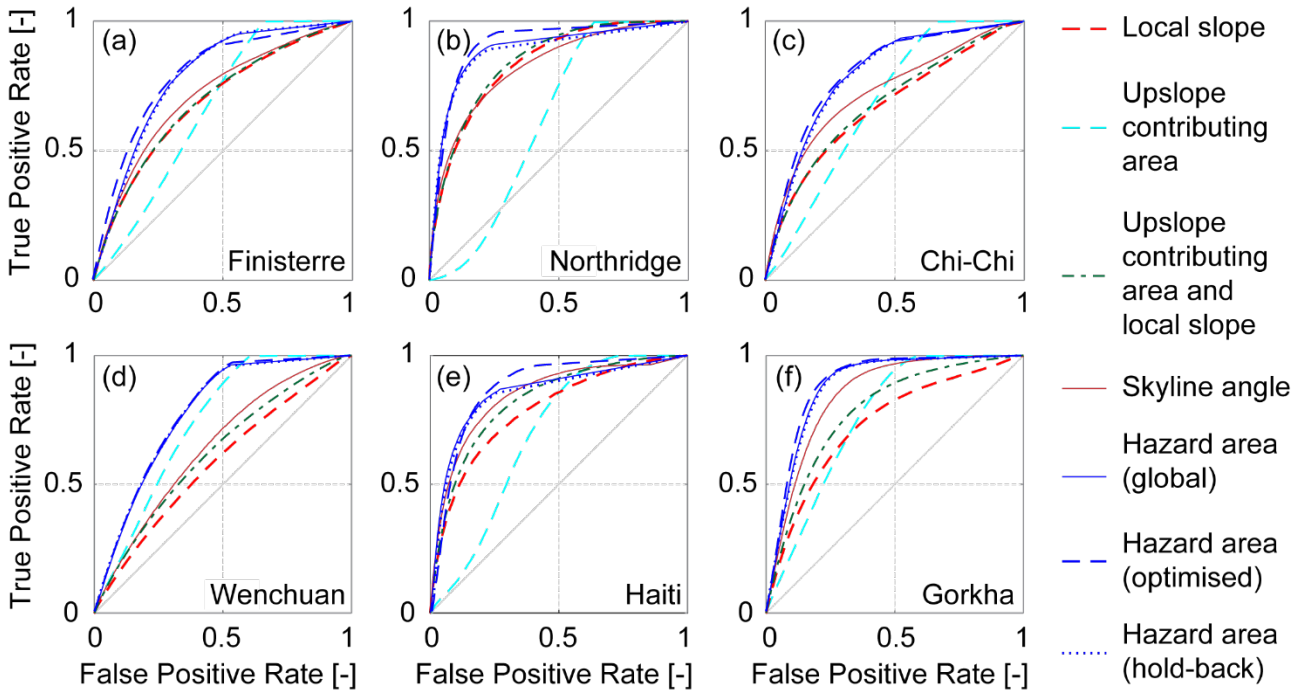

Figure S2: Receiver operating characteristic (ROC) curves for the six landslide inventories and five metrics examined here, as shown in Figure 6 of the paper, but with the addition of ROC curves for hazard area with (1) site-specific optimised parameters and (2) hold-back parameters (i.e., global averages from five sites excluding the test site). The six inventories are: a) Finisterre, b) Northridge, c) Chi-Chi, d) Wenchuan, e) Haiti, f) Gorkha. False positive rate is given by the number of false positives divided by the sum of false positives and true negatives. True positive rate is given by the number of true positives divided by the sum of true positives and false negatives. The 1:1 line represents the naïve (random) case. Curves plotting closer to the top left corner of each panel represent better model performance.

Supplementary Information 2: Table S2. Study site characteristics

	Northridge	Finisterre	Chi-Chi	Wenchuan	Haiti	Gorkha
Geology	Weakly cemented sedimentary rocks[1].	Volcaniclastic & volcanic rocks thrust over coarse-grained foreland deposits capped by limestones [9]	Neogene sediments and older metasedimentary rocks [15]	Granitic massifs, a passive margin sequence, and a thick foreland basin succession [22]	Sub-parallel belts of igneous, metamorphic and sedimentary rocks [28]	Variably metamorphosed sedimentary and igneous rocks, some sedimentary metasedimentary [33]
Denudation rates	0.1-1 mm/yr[2]	up to 0.3 mm/yr [10]	3-7 mm/yr [16]	0.5 mm/yr [23]		0.3-3 mm/yr [34]
Koppen climate classification	Warm-summer Mediterranean.[3]	Tropical [3]	Humid subtropical[3]	Humid subtropical[3]	Tropical [3]	Humid subtropical[3]
Temperature	1-18 ˚C [4]	26-27 ˚C [11]	22 ˚C [17]	15-17 °C [24]	25˚C [29]	-6-18 ˚C [35]
Annual precipitation	0.3–0.9 m [5]	2.5 - 4 m [11]	2.5 m [17]	0.6 - 1.1 m [24]	~1.2 m [29]	0.5 - 3 m [35]
Vegetation	annual grassland, sage scrub, and chaparral with some piñon-juniper, oak and pine woodlands. [6]	tropical wet or tropical montane evergreen forest some sub-alpine grasslands. [12]	Subtropical moist broadleaf forests [18]	montane broad-leaved and conifer forest with some alpine shrub and steppe [25]	moist broadleaf forest some pine or dry broadleaf forest, with some savannah [19,30]	temperate broadleaf and coniferous forests with some alpine tundra [36]
Earthquake agnitude	M_w 6.7	M_w 6.9 & M_w 6.7	M_w 7.6	M_w 7.9	M_w 7.0	M_w 7.8 & M_w 7.2
Date	17/1/1994	13/10/93 & 25/10/93	21/9/1999	12/5/2008	12/1/2010	25/4/15 & 12/5/15
Focal depth	19 km [7]	25 km & 30 km [13]	8–10 km [19]	14-19 km [26]	13 km [31]	8.2 km [37]
Mapped landslides	11,111 [8]	4,790 [14]	9,272 [21]	18,824 of 69,606 [27]	23,567 [32]	24,915 [38]
Study area	4,000 km^2	4,300 km^2	10,500 km^2	9,800 of 38,000 km^2	3,800 km^2	29,000 km^2
Landslide mapping	field & aerial reconnaissance, manually digitized on 1:24,000 maps [8]	30 m SPOT images[14]	20 m SPOT images [21]	high-resolution (<15 m) satellite images and air photos [27]	satellite imagery with a resolution 0.6 m [32]	<0.5 m Worldview-2 Worldview-3 & Pleiades images [38]

Citations: [1] Colburn et al., 1981; Tsutsumi and Yeats, 1999; Parise and Jibson, 2000; [2] Meigs et al., 1999; Lave and Burbank, 2004; [3] Peel et al., 2007; [4] NOAA, 2017; [5] National Atlas of United States, 2011; [6] Griffith et al., 2016; [7] Hauksson et al., 1995; [8] Harp and Jibson, 1996; [9] Davies et al., 1987; Abbott et al., 1994; [10] Abbott et al., 1997; [11] Hovius et al., 1998; [12] MacKinnon 1997; Paijmans 1975; [13] Stevens et al., 1998; [14] Meunier et al., 2007; [15] Lin et al., 2000; [16] Dadson et al., 2003; [17] Wu and Kuo, 1999; [18] Olsen et al., 2001; [19] Shin and Teng, 2001; [20] Lee et al., 2001; [21] Dadson et al., 2004; [22] Burchfiel et al., 1995; [23] Ouimet et al., 2009; Godard et al., 2010; Liu-Zeng et al., 2011; [24] Liu-Zeng et al., 2011; Li et al., 2016; [25] Yu et al., 2001; [26] Li et al., 2008; [27] Li et al., 2014; [28] Sen et al., 1988, Escuder-Viruete et al., 2007; [29] Gorum et al., 2013; Libohova et al., 2017; [30] Churches et al., 2014; [31] Mercier de Lépinay et al., 2011; [32] Harp et al., 2016; [33] Hodges et al., 1996; Searle and Godin, 2003; Craddock et al., 2007; [34] Lupker et al., 2012; Godard et al., 2014; [35] Bookhagen and Burbank, 2006; [36] Singh and Singh, 1987; [37] Hayes et al., 2015; [38] Roback et al., 2018

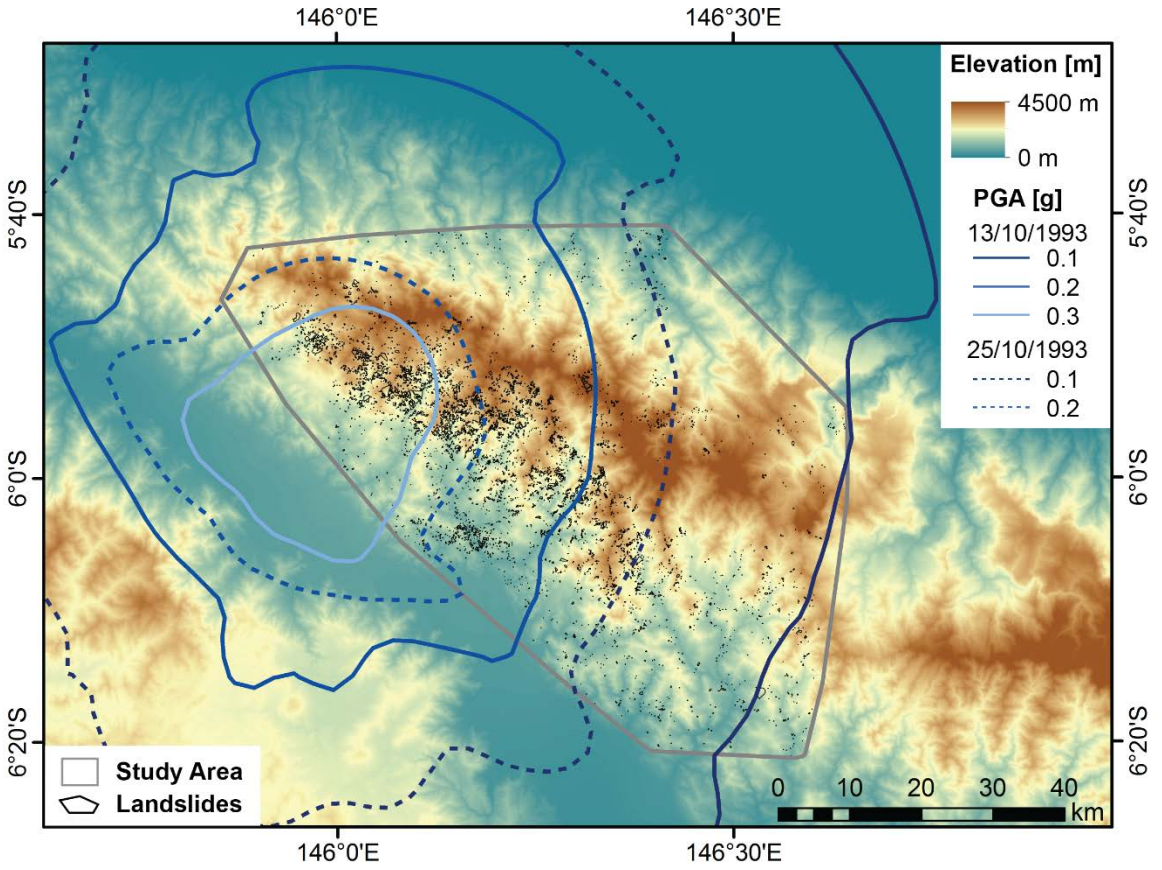

Figure S3: Finisterre study area with PGA contours from USGS shakemap for the 13th and 25th October 1993 earthquakes, elevation from 1 arcsecond SRTM and landslides from Meunier et al. (2007).

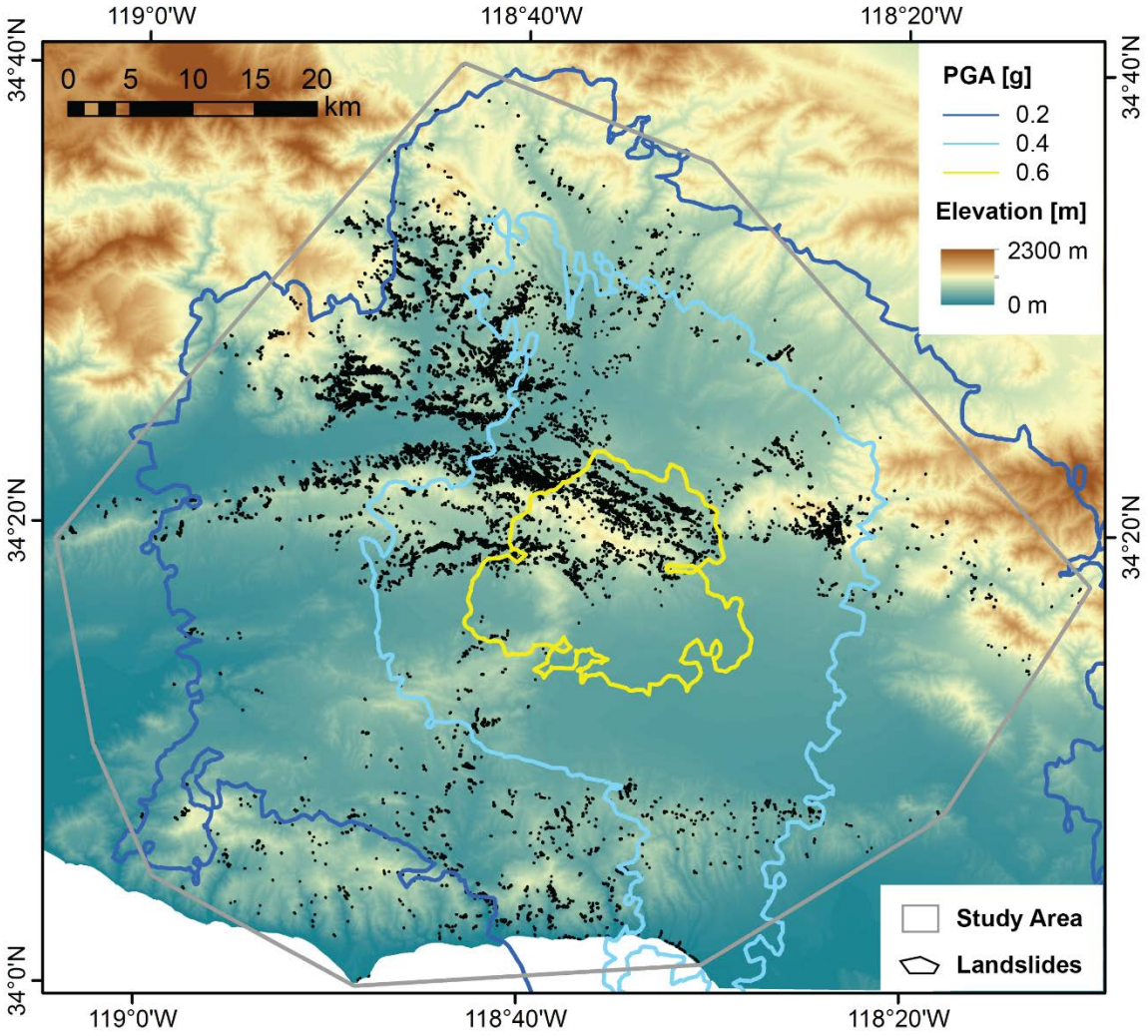

Figure S4: Northridge study area with PGA contours from USGS shakemap, Elevation from 10 m NED and landslides from Harp and Jibson (1996).

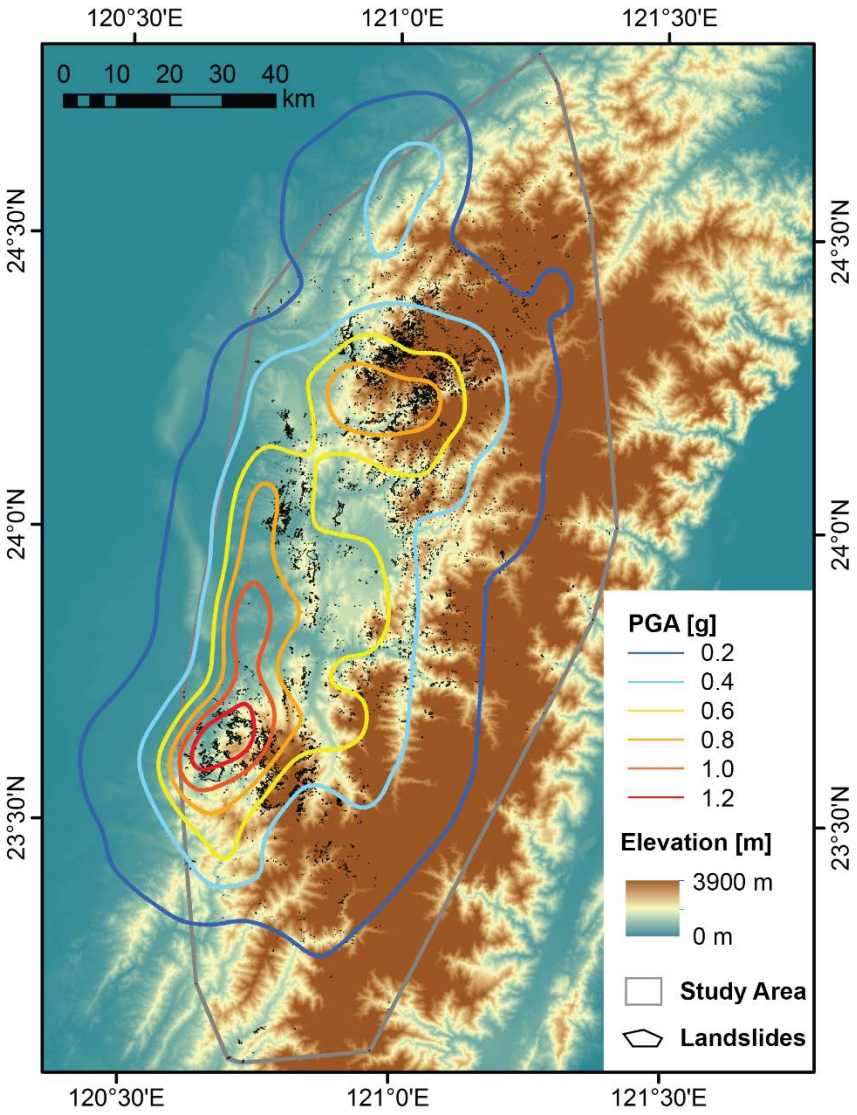

Figure S5: Chi-Chi study area with PGA contours from USGS shakemap, elevation from 1 arcsecond SRTM and landslides from Dadson et al. (2004).

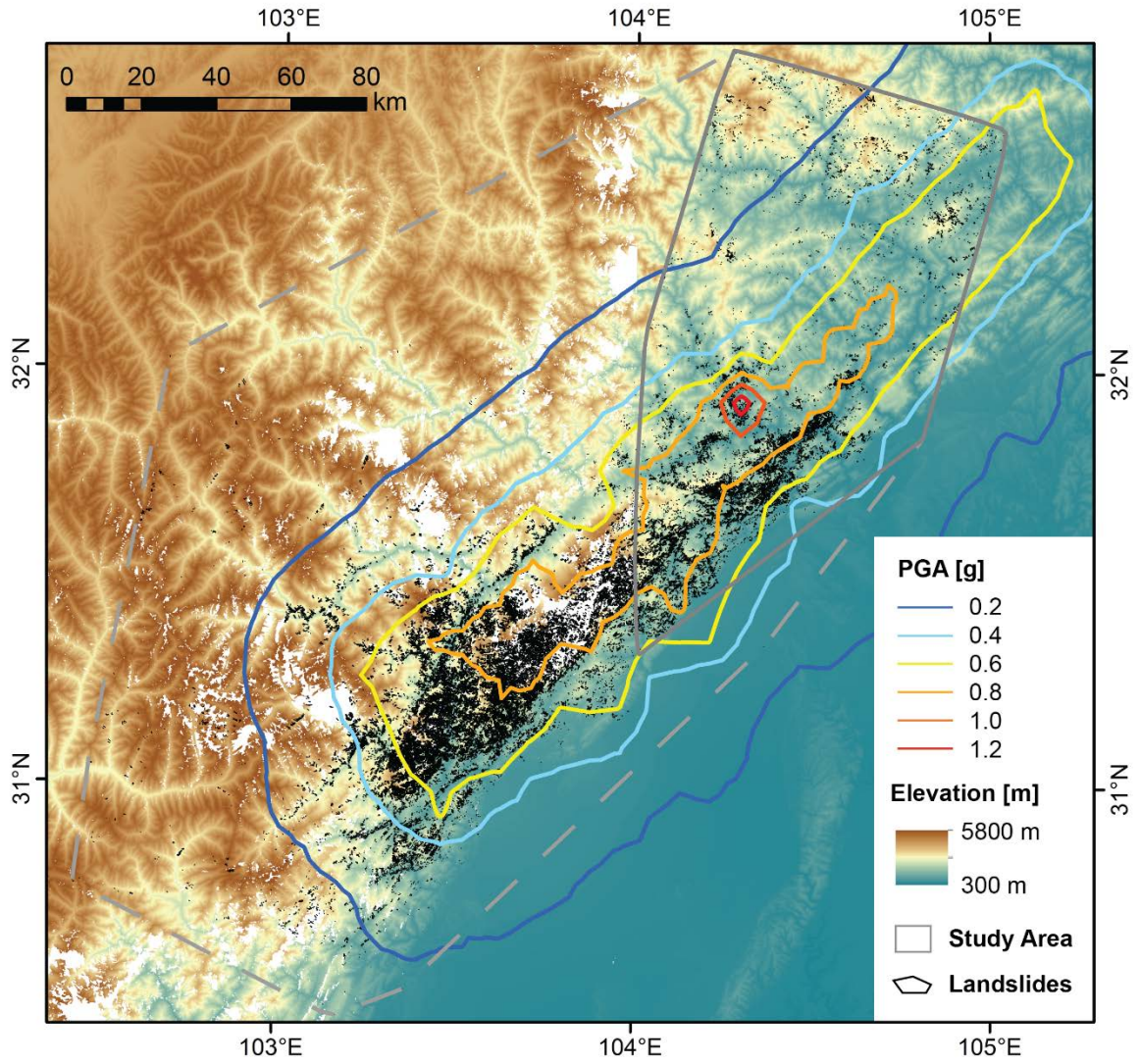

77

78 Figure S6: Wenchuan study area with PGA contours from USGS shakemap, Elevation from 1 arc second
79 SRTM and landslides from Li et al. (2014). The dashed grey line shows a convex hull around the full
80 inventory of landslides mapped by Li et al. the solid grey line indicates the study area used in this article.
81 The study area was chosen to avoid the large gaps in the 1 arcsecond SRTM data (white patches above).

82

83

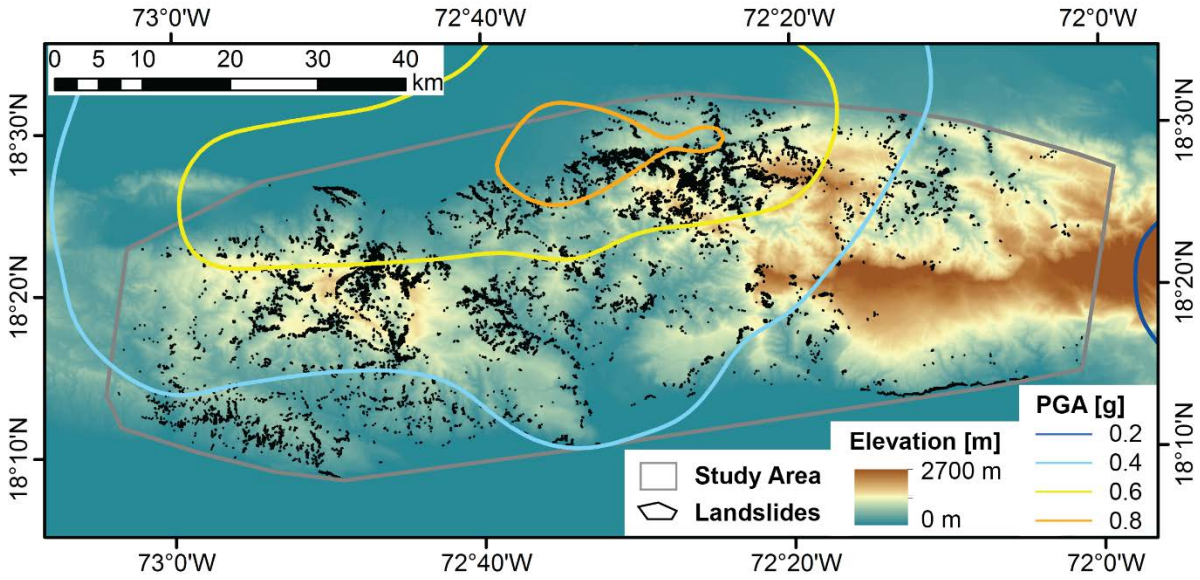

84

85 Figure S7: Haiti study area with PGA contours from USGS shakemap, elevation from 1 arcsecond SRTM and
86 landslides from Harp et al. (2016).

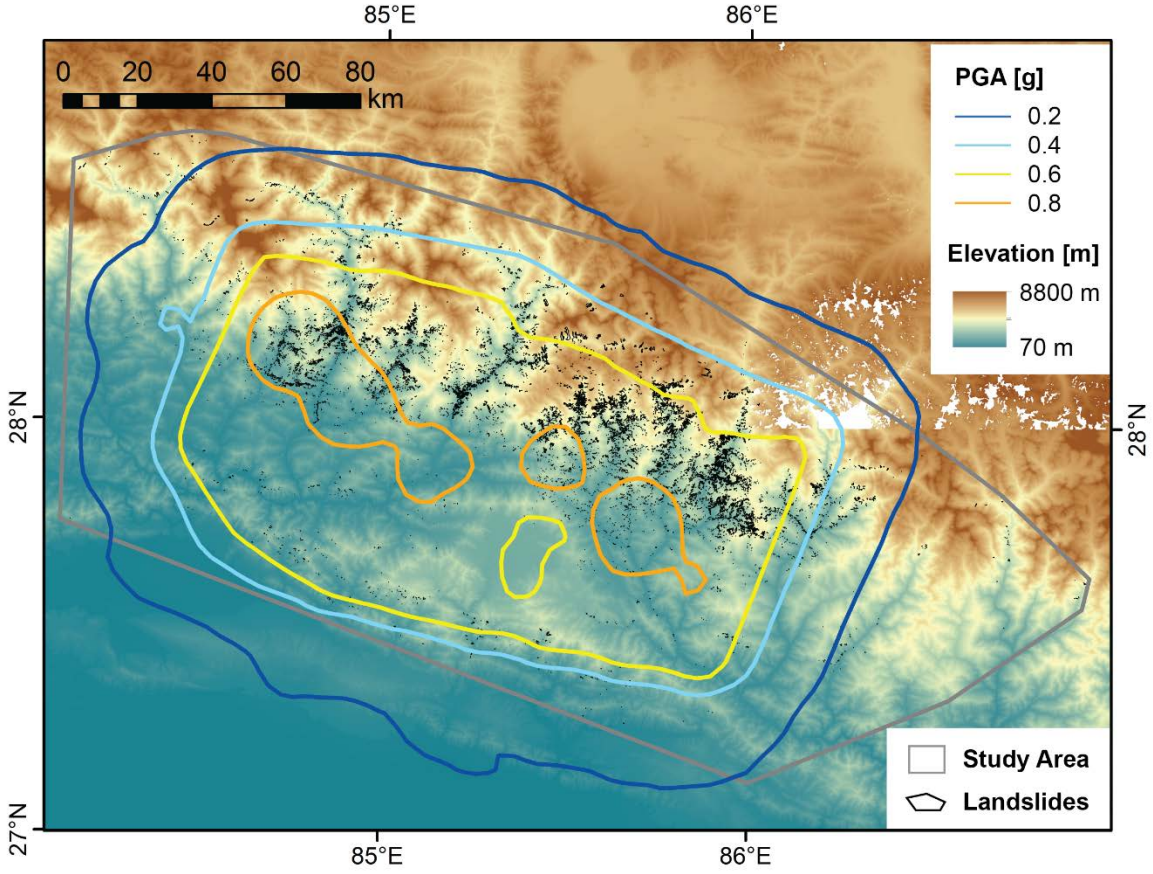

87 Figure
88 S8: Gorkha study area with PGA contours from USGS shakemap for the 25th April 2015 Gorkha earthquake,
89 elevation from 1 arcsecond SRTM and landslides from Roback et al. (2018).

90

Supplementary Information 3: Normalised results for slope and upslope contributing area in combination

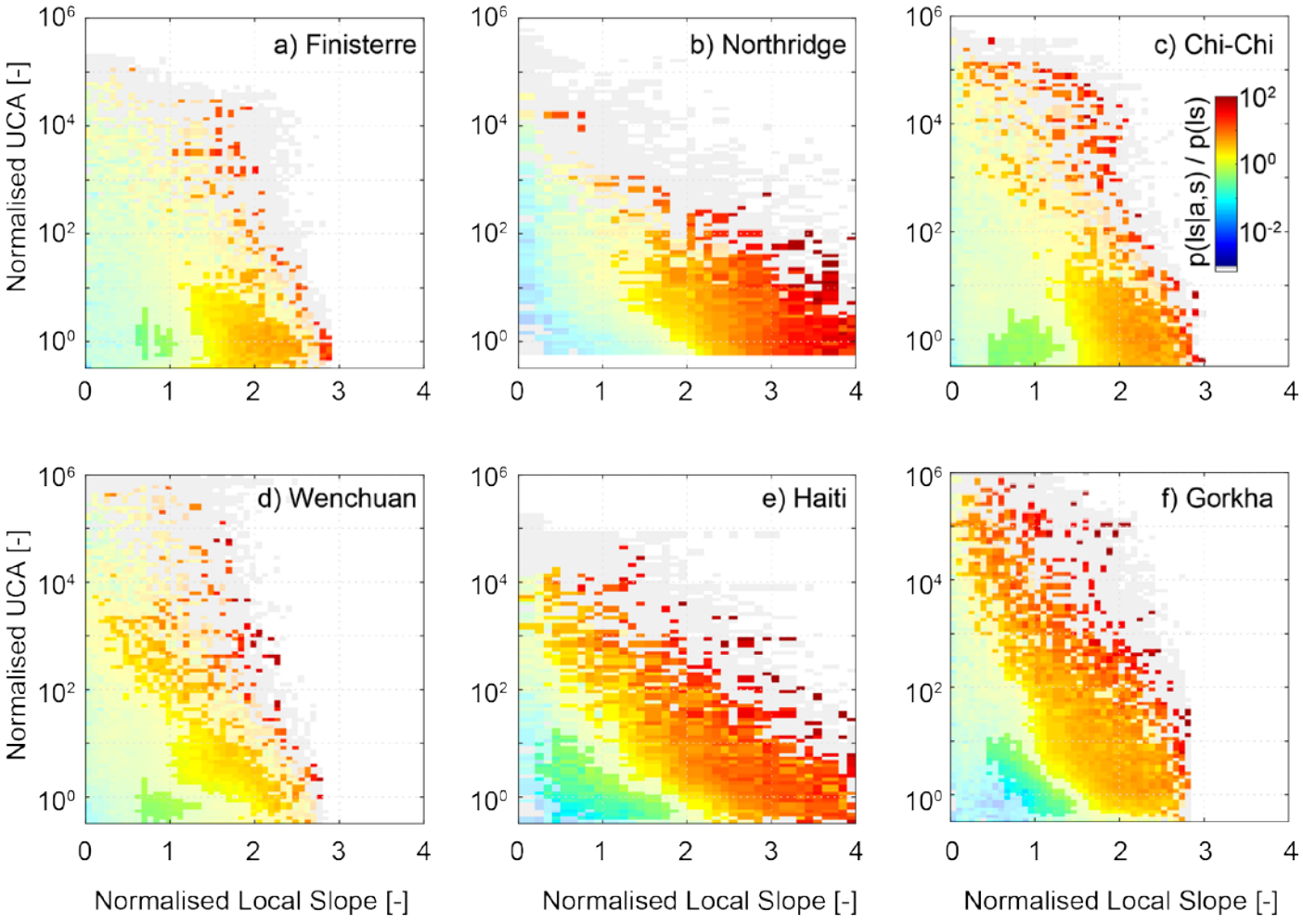

Figure S9. Two-dimensional plots of landslide hazard, defined as conditional landslide probability $P(L|s,a)$ normalised by study area average landslide probability $P(L)$, where s is local slope normalised by the study area average slope and a is upslope contributing area normalised by the upslope contributing area at which channels begin. Grey cells indicate slope-area pairs with data but with no cells touching a landslide. Fainter colours indicate landslide hazard estimates that do not differ significantly from the study area average.

Supplementary Information 4: Impact of landslide inventory uncertainty and DEM resolution

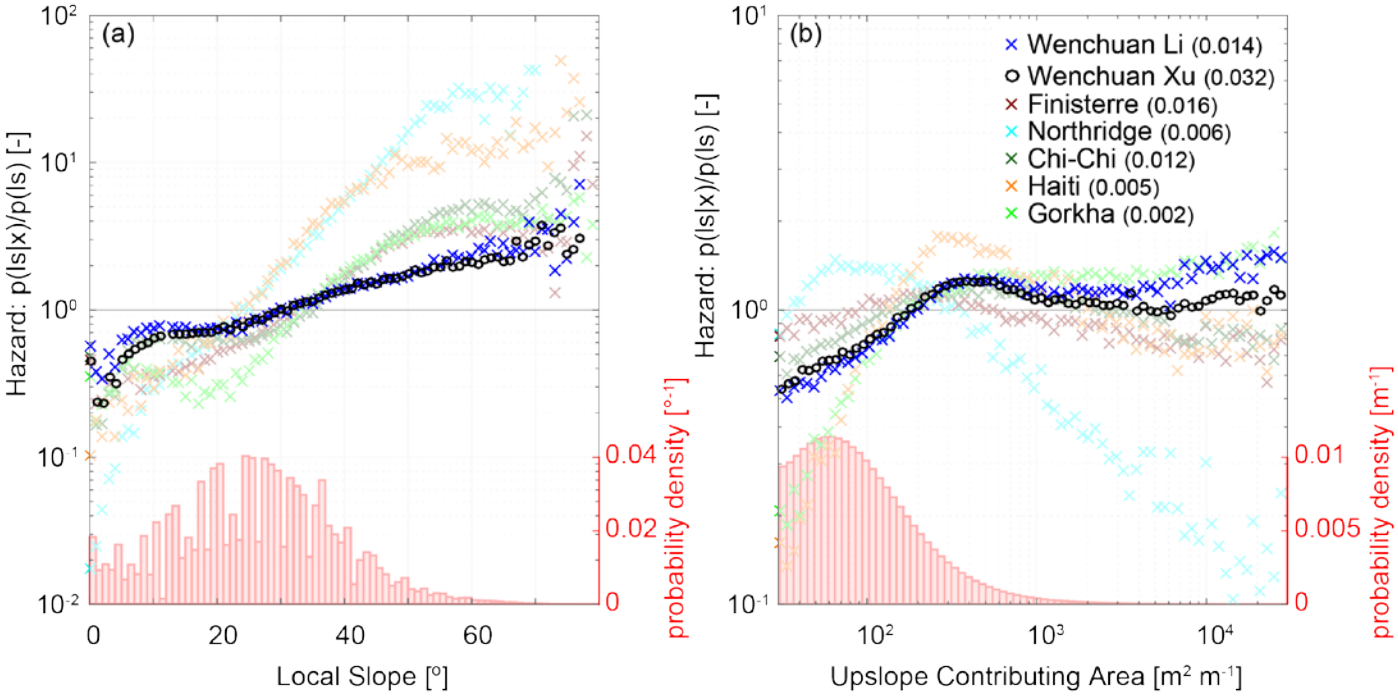

Figure S10. Comparing the impact of different landslide inventories. Landslide hazard is defined as $P(L|x) / P(L)$ and is estimated from two different landslide inventories for the Wenchuan earthquake, where x is a) local slope, and b) upslope contributing area per unit contour length. Numbers in brackets show study area average landslide probabilities. Results from other earthquakes are shown in faint colours for context. The results from Li et al. (2014) and Xu et al. (2014) for the Wenchuan earthquake are strongly similar.

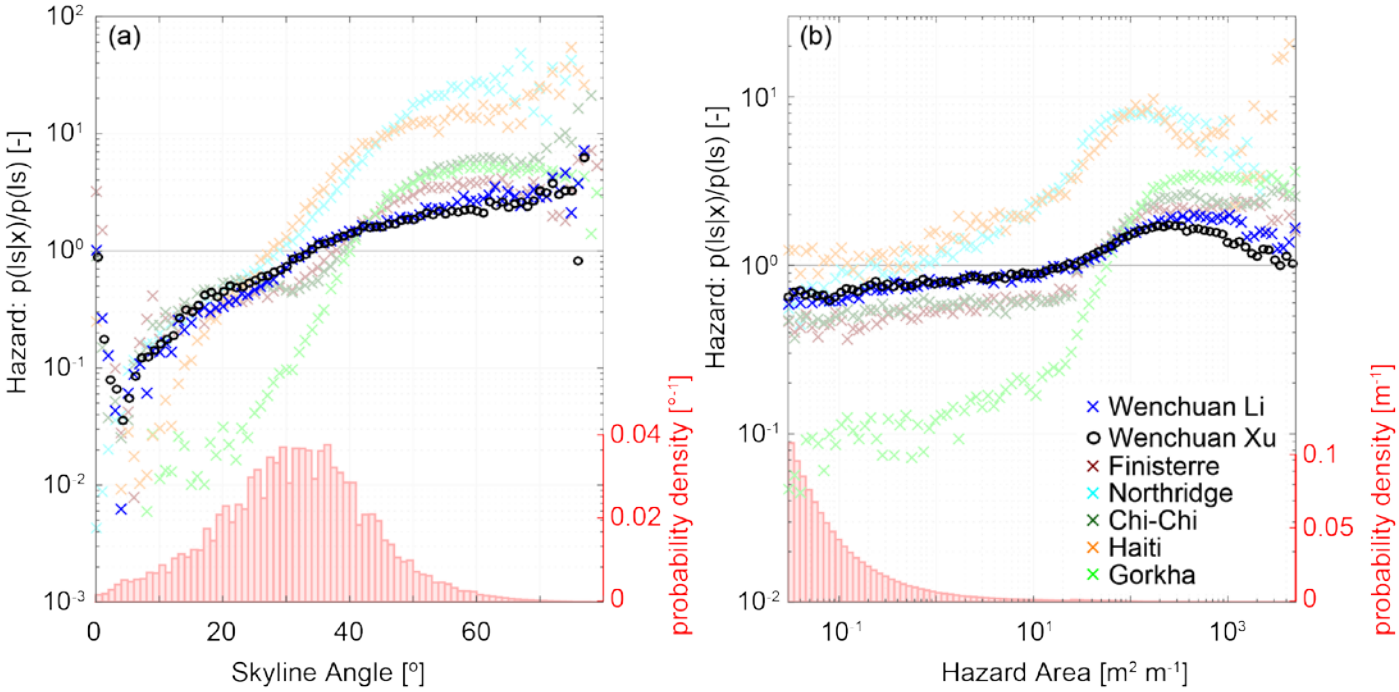

112

113 **Figure S11**. Comparing the impact of different landslide inventories. Landslide hazard is defined
114 as $P(L|x) / P(L)$ and is estimated from two different landslide inventories for the Wenchuan
115 earthquake, where x is a) skyline angle and b) upslope contributing area per unit contour length.
116 Red bars show histograms of skyline angle and hazard area over the six inventories. Results from
117 other earthquakes are shown in faint colours for context. The results from Li et al. (2014) and Xu et
118 al. (2014) for the Wenchuan earthquake are strongly similar.

119 **Table S3.** Area under the ROC curve for the five hazard metrics over the six coseismic landslide
120 inventories. The best performing metric for each inventory is in bold, the second best is in italics.

	Hazard area	Skyline angle	Slope + upslope contributing area	Local slope	Upslope contributing area
Northridge 10	**0.91**	**0.91**	0.86	0.85	0.63
Northridge 20	**0.91**	*0.88*	0.86	0.85	0.63
Northridge 30 (NED DEM)	**0.89**	0.83	*0.84*	*0.84*	0.62
Northridge 30 (SRTM DEM)	0.66	**0.83**	**0.83**	**0.83**	0.64
Northridge 60	**0.83**	*0.80*	*0.80*	*0.80*	0.62
Northridge 90	0.75	0.77	**0.78**	**0.78**	0.61
Wenchuan Li et al	**0.78**	0.65	0.62	0.58	*0.74*
Wenchuan Xu et al	**0.76**	0.63	0.62	0.59	*0.73*

121

References

Abbott, L.D., Silver, E.A., Anderson, R.S., Smith, R., Ingle, J.C., Kling, S.A., Haig, D., Small, E., Galewsky, J. and Sliter, W.S.: Measurement of tectonic surface uplift rate in a young collisional mountain belt. *Nature*, *385*(6616), pp.501-507. 1997.

Bookhagen, B. and Burbank, D.W.: Topography, relief, and TRMM-derived rainfall variations along the Himalaya. *Geophysical Research Letters*, *33*(8). 2006.

Burchfiel, B.C., Zhiliang, C., Yupinc, L. and Royden, L.H.: Tectonics of the Longmen Shan and adjacent regions, central China. *International Geology Review*, *37*(8), pp.661-735. 1995.

Churches, C.E., Wampler, P.J., Sun, W. and Smith, A.J.: Evaluation of forest cover estimates for Haiti using supervised classification of Landsat data. *International Journal of Applied Earth Observation and Geoinformation*, *30*, pp.203-216. 2014.

Colburn, I.P., Saul, L.E.R. and Almgren, A.A.: The Chatsworth Formation: a new formation name for the Upper Cretaceous strata of the Simi Hills, California. 1981.

Craddock, W.H., Burbank, D.W., Bookhagen, B. and Gabet, E.J.: Bedrock channel geometry along an orographic rainfall gradient in the upper Marsyandi River valley in central Nepal. *Journal of Geophysical Research: Earth Surface*, *112*(F3). 2007.

Dadson, S.J., Hovius, N., Chen, H., Dade, W.B., Hsieh, M.L., Willett, S.D., Hu, J.C., Horng, M.J., Chen, M.C., Stark, C.P. and Lague, D.: Links between erosion, runoff variability and seismicity in the Taiwan orogen. *Nature*, *426*(6967), pp.648-651. 2003.

Davies, H.L., Lock, J., Tiffin, D.L., Honza, E., Okuda, Y., Murakami, F. and Kisimoto, K.: Convergent tectonics in the Huon Peninsula region, Papua New Guinea. *Geo-Marine Letters*, *7*(3), pp.143-152. 1987.

Escuder-Viruete, J., Pérez-Estaún, A., Contreras, F., Joubert, M., Weis, D., Ullrich, T.D. and Spadea, P.: Plume mantle source heterogeneity through time: Insights from the Duarte Complex, Hispaniola, northeastern Caribbean. *Journal of Geophysical Research: Solid Earth*, *112*(B4). 2007.

Godard, V., Lavé, J., Carcaillet, J., Cattin, R., Bourlès, D. and Zhu, J.: Spatial distribution of denudation in Eastern Tibet and regressive erosion of plateau margins. *Tectonophysics*, *491*(1), pp.253-274. 2010.

Godard, V., Bourlès, D.L., Spinabella, F., Burbank, D.W., Bookhagen, B., Fisher, G.B., Moulin, A. and Léanni, L.: Dominance of tectonics over climate in Himalayan denudation. *Geology*, *42*(3), pp.243-246. 2014.

Gorum, T., van Westen, C.J., Korup, O., van der Meijde, M., Fan, X. and van der Meer, F.D.: Complex rupture mechanism and topography control symmetry of mass-wasting pattern, 2010 Haiti earthquake. *Geomorphology*, *184*, pp.127-138. 2013.

Griffith, G.E., Omernik, J.M., Smith, D.W., Cook, T.D., Tallyn, E., Moseley, K., and Johnson, C.B.: Ecoregions of California (poster): U.S. Geological Survey Open-File Report 2016–1021, with map, scale 1:1,100,000, http://dx.doi.org/10.3133/ofr20161021. 2016.

Harp, E.L. and Jibson, R.W.: Landslides triggered by the 1994 Northridge, California, earthquake. *Bulletin of the Seismological Society of America*, *86*(1B), pp.S319-S332. 1996.

Harp, E.L., Jibson, R.W., and Schmitt, R.G.: Map of landslides triggered by the January 12, 2010, Haiti earthquake: U.S. Geological Survey Scientific Investigations Map 3353, 15 p., 1 sheet, scale 1:150,000, http://dx.doi.org/10.3133/sim3353. 2016.

Hauksson, E., Jones, L.M. and Hutton, K.: The 1994 Northridge earthquake sequence in California: Seismological and tectonic aspects. *Journal of Geophysical Research: Solid Earth*, *100*(B7), pp.12335-12355. 1995.

Hayes, G.P., Briggs, R.W., Barnhart, W.D., Yeck, W.L., McNamara, D.E., Wald, D.J., Nealy, J.L., Benz, H.M., Gold, R.D., Jaiswal, K.S. and Marano, K.: Rapid characterization of the 2015 M w 7.8 Gorkha, Nepal, earthquake sequence and its seismotectonic context. *Seismological Research Letters*, *86*(6), pp.1557-1567. 2015.

Hodges, K.V., Parrish, R.R. and Searle, M.P. Tectonic evolution of the central Annapurna range, Nepalese Himalayas. *Tectonics*, *15*(6), pp.1264-1291. 1996.

Hovius, N., Stark, C.P., Tutton, M.A. and Abbott, L.D.: Landslide-driven drainage network evolution in a pre-steady-state mountain belt: Finisterre Mountains, Papua New Guinea. *Geology*, *26*(12), pp.1071-1074. 1998.

Lavé, J. and Burbank, D.: Denudation processes and rates in the Transverse Ranges, southern California: Erosional response of a transitional landscape to external and anthropogenic forcing. *Journal of Geophysical Research: Earth Surface*, *109*(F1). 2004.

Lee, W.H.K., Shin, T.C., Kuo, K.W., Chen, K.C. and Wu, C.F.: CWB free-field strong-motion data from the 21 September Chi-Chi, Taiwan, earthquake. *Bulletin of the seismological society of America*, *91*(5), pp.1370-1376. 2001.

Li, X., Zhou, Z., Yu, H., Wen, R., Lu, D., Huang, M., Zhou, Y. and Cu, J.: Strong motion observations and recordings from the great Wenchuan Earthquake. *Earthquake Engineering and Engineering Vibration*, *7*(3), pp.235-246. 2008.

Li, G., West, A.J., Densmore, A.L., Jin, Z., Parker, R.N. and Hilton, R.G.: Seismic mountain building: Landslides associated with the 2008 Wenchuan earthquake in the context of a generalized model for earthquake volume balance. *Geochemistry, Geophysics, Geosystems*, *15*(4), pp.833-844. 2014.

Li, G., West, A.J., Densmore, A.L., Hammond, D.E., Jin, Z., Zhang, F., Wang, J. and Hilton, R.G.: Connectivity of earthquake-triggered landslides with the fluvial network: Implications for landslide sediment transport after the 2008 Wenchuan earthquake. *Journal of Geophysical Research: Earth Surface*, *121*(4), pp.703-724. 2016.

Libohova, Z., Wysocki, D., Schoeneberger, P., Reinsch, T., Kome, C., Rolfes, T., Jones, N., Monteith, S. and Matos, M.: Soils and climate of Cul de Sac Valley, Haiti: A soil water and geomorphology perspective. *Journal of Soil and Water Conservation*, *72*(2), pp.91-101. 2017.

Lin, G.W., Chen, H., Hovius, N., Horng, M.J., Dadson, S., Meunier, P. and Lines, M.: Effects of earthquake and cyclone sequencing on landsliding and fluvial sediment transfer in a mountain catchment. *Earth Surface Processes and Landforms*, *33*(9), pp.1354-1373. 2008.

Liu-Zeng, J., Wen, L., Oskin, M. and Zeng, L.: Focused modern denudation of the Longmen Shan margin, eastern Tibetan Plateau. *Geochemistry, Geophysics, Geosystems*, *12*(11). 2011.

Lupker, M., Blard, P.H., Lave, J., France-Lanord, C., Leanni, L., Puchol, N., Charreau, J. and Bourlès, D.: 10 Be-derived Himalayan denudation rates and sediment budgets in the Ganga basin. *Earth and Planetary Science Letters*, *333*, pp.146-156. 2012.

MacKinnon, J.R. ed.: *Protected areas systems review of the Indo-Malayan realm*. Asian Bureau for Conservation. 1997.

Meigs, A., Brozovic, N. and Johnson, M.L.: Steady, balanced rates of uplift and erosion of the Santa Monica Mountains, California. *Basin Research*, *11*(1), pp.59-73. 1999.

Mercier de Lépinay, B.M., Deschamps, A., Klingelhoefer, F., Mazabraud, Y., Delouis, B., Clouard, V., Hello, Y., Crozon, J., Marcaillou, B., Graindorge, D. and Vallée, M.: The 2010 Haiti earthquake: A complex fault pattern constrained by seismologic and tectonic observations. *Geophysical Research Letters*, *38*(22). 2011.

Meunier, P., Hovius, N. and Haines, A.J.: Regional patterns of earthquake-triggered landslides and their relation to ground motion. *Geophysical Research Letters*, *34*(20). 2007.

National Atlas of the United States: *United States Average Annual Precipitation, 1990-2009, Map*, Reston, VA. https://catalog.data.gov/dataset/united-states-average-annual-precipitation-1990-2009-direct-download. 2011.

NOAA: Online Weather Data: http://w2.weather.gov/climate/xmacis.php?wfo=sgx. *National Oceanic and Atmospheric Administration. Retrieved 2017-10-30. 2017.*

Olson, D.M., Dinerstein, E., Wikramanayake, E.D., Burgess, N.D., Powell, G.V., Underwood, E.C., D'amico, J.A., Itoua, I., Strand, H.E., Morrison, J.C. and Loucks, C.J.: Terrestrial Ecoregions of the World: A New Map of Life on Earth A new global map of terrestrial ecoregions provides an innovative tool for conserving biodiversity. *BioScience*, *51*(11), pp.933-938. 2001.

Ouimet, W.B., Whipple, K.X. and Granger, D.E.: Beyond threshold hillslopes: Channel adjustment to base-level fall in tectonically active mountain ranges. *Geology*, *37*(7), pp.579-582. 2009.

Paijmans, K., 1975. Explanatory notes to the vegetation map of Papua New Guinea.

Parise, M. and Jibson, R.W.: A seismic landslide susceptibility rating of geologic units based on analysis of characteristics of landslides triggered by the 17 January, 1994 Northridge, California earthquake. *Engineering geology*, *58*(3), pp.251-270. 2000.

Peel, M.C., Finlayson, B.L. and McMahon, T.A.: Updated world map of the Köppen-Geiger climate classification. *Hydrology and earth system sciences discussions*, *4*(2), pp.439-473. 2007.

Roback, K., Clark, M.K., West, A.J., Zekkos, D., Li, G., Gallen, S.F., Chamlagain, D. and Godt, J.W.: The size, distribution, and mobility of landslides caused by the 2015 M w 7.8 Gorkha earthquake, Nepal. *Geomorphology*. 2018.

Searle, M.P. and Godin, L.: The South Tibetan detachment and the Manaslu leucogranite: A structural reinterpretation and restoration of the Annapurna-Manaslu Himalaya, Nepal. *The Journal of Geology*, *111*(5), pp.505-523. 2003.

Sen, G., Hickey-Vargas, R., Waggoner, D.G. and Maurrasse, F.: Geochemistry of basalts from the Dumisseau Formation, southern Haiti: implications for the origin of the Caribbean Sea crust. *Earth and Planetary Science Letters*, *87*(4), pp.423-437. 1988.

Shin, T.C. and Teng, T.L.: An overview of the 1999 Chi-Chi, Taiwan, earthquake. *Bulletin of the Seismological Society of America*, *91*(5), pp.895-913. 2001.

Singh, J.S. and Singh, S.P.: Forest vegetation of the Himalaya. *The Botanical Review*, *53*(1), pp.80-192. 1987.

Stevens, C., McCaffrey, R., Silver, E.A., Sombo, Z., English, P. and Van der Kevie, J.: Mid-crustal detachment and ramp faulting in the Markham Valley, Papua New Guinea. *Geology*, *26*(9), pp.847-850. 1998.

Tsutsumi, H. and Yeats, R.S.: Tectonic setting of the 1971 Sylmar and 1994 Northridge earthquakes in the San Fernando Valley, California. *Bulletin of the Seismological Society of America*, *89*(5), pp.1232-1249. 1999.

Wu, C.C. and Kuo, Y.H.: Typhoons affecting Taiwan: Current understanding and future challenges. *Bulletin of the American Meteorological Society*, *80*(1), pp.67-80. 1999.

Yu, G., Tang, L., Yang, X., Ke, X. and Harrison, S.P.: Modern pollen samples from alpine vegetation on the Tibetan Plateau. *Global Ecology and Biogeography*, *10*(5), pp.503-519. 2001.